



RESEARCH ARTICLE

10.1002/2016JD025599

Key Points:

- A ray theory-based model for lightning sferics in Earth-ionosphere waveguide is proposed and tested with measured data
- The model can be used to retrieve the ionosphere feature from lightning sferics or to predict the sferic feature of a lightning discharge
- Both simulation and observation show there is magneto-ionic splitting phenomenon in the lower ionosphere for lightning sferic at night

Correspondence to:

M. Chen,
mingli.chen@polyu.edu.hk

Citation:

Qin, Z., M. Chen, B. Zhu, and Y. Du (2017), An improved ray theory and transfer matrix method-based model for lightning electromagnetic pulses propagating in Earth-ionosphere waveguide and its applications, *J. Geophys. Res. Atmos.*, 122, 712–727, doi:10.1002/2016JD025599.

Received 30 JUN 2016

Accepted 6 JAN 2017

Accepted article online 7 JAN 2017

Published online 21 JAN 2017

The copyright line for this article was changed on 22 AUG 2017 after original online publication.

©2017. The Authors.

This is an open access article under the terms of the Creative Commons Attribution-NonCommercial-NoDerivs License, which permits use and distribution in any medium, provided the original work is properly cited, the use is non-commercial and no modifications or adaptations are made.

An improved ray theory and transfer matrix method-based model for lightning electromagnetic pulses propagating in Earth-ionosphere waveguide and its applications

Zilong Qin¹ , Mingli Chen¹ , Baoyou Zhu², and Ya-ping Du¹

¹Department of Building Service Engineering, Hong Kong Polytechnic University, Hong Kong, ²CAS Key Laboratory of Geospace Environment, School of Earth and Space Sciences, University of Science and Technology of China, Hefei, China

Abstract An improved ray theory and transfer matrix method-based model for a lightning electromagnetic pulse (LEMP) propagating in Earth-ionosphere waveguide (EIWG) is proposed and tested. The model involves the presentation of a lightning source, parameterization of the lower ionosphere, derivation of a transfer function representing all effects of EIWG on LEMP sky wave, and determination of attenuation mode of the LEMP ground wave. The lightning source is simplified as an electric point dipole standing on Earth surface with finite conductance. The transfer function for the sky wave is derived based on ray theory and transfer matrix method. The attenuation mode for the ground wave is solved from Fock's diffraction equations. The model is then applied to several lightning sferics observed in central China during day and night times within 1000 km. The results show that the model can precisely predict the time domain sky wave for all these observed lightning sferics. Both simulations and observations show that the lightning sferics in nighttime has a more complicated waveform than in daytime. Particularly, when a LEMP propagates from east to west ($\Phi = 270^\circ$) and in nighttime, its sky wave tends to be a double-peak waveform (dispersed sky wave) rather than a single peak one. Such a dispersed sky wave in nighttime may be attributed to the magneto-ionic splitting phenomenon in the lower ionosphere. The model provides us an efficient way for retrieving the electron density profile of the lower ionosphere and hence to monitor its spatial and temporal variations via lightning sferics.

1. Introduction

Lightning is the most intensive discharge process that occurs frequently in the terrestrial space. It emits a wide band of electromagnetic waves ranging from several hertz to a few gigahertz with the main power concentrating at very low frequency (3–30 kHz, VLF) and low frequency (30–300 kHz, LF) bands, namely a lightning electromagnetic pulse (LEMP). On the other side, the lower ionosphere, the *D/E* region has an extremely low electron density and a high electron-neutral collision rate, which forms a damping plasma region that can interfere with ELF/VLF waves. Hence, LEMP can be an efficient tool to probe the variation of lower ionosphere via its interference with the lower ionosphere. To achieve this, a model that describes accurately the characteristics of LEMP propagating in the Earth-ionosphere waveguide (EIWG) is essential.

Most previous works on EIWG model were derived from the mode theory [Budden, 1961; Galejs, 2013; Wait, 2013]. The mode theory calculates infinite number of independent wave modes between the source and receiver according to the properties of top and bottom boundaries of EIWG. The field at the receiver is the summation of fields from these modes. A widely used mode theory-based EIWG computing program named Long Wave Propagation Code (LWPC) was firstly developed by the United States Navy [Ferguson *et al.*, 1989]. With a modified LWPC, many researchers succeeded in retrieving the average electron density profile of ionosphere *D* region in an area through LEMPs [Cummer *et al.*, 1998; Cummer, 2000; Cummer and Inan, 2000; Cheng and Cummer, 2005; Cheng *et al.*, 2006]. Relied on the phase and amplitude predicted by LWPC, the characteristics of variation of the ionosphere *D* region were also investigated through radios [Thomson and Clilverd, 2000; Thomson *et al.*, 2007; Thomson and McRae, 2009; Thomson, 2010].

In recent years, an improved 2-D cylindrical finite difference time domain (FDTD) model for LEMP propagating in EIWG was established by the Duke group [Hu and Cummer, 2006]. With this model they studied the characteristics of electron density distribution of ionosphere *D* region versus X-ray flux density during daytime and nighttime at midlatitude region [Han and Cummer, 2010a, 2010b; Han *et al.*, 2011]. Another

3-D spherical FDTD model was developed to investigate the heating effect of radio and lightning events below the ionosphere [Marshall, 2012]. The HF-heating effect in the ionosphere and the reflection and penetration waves of a HF transmitter were investigated with a mode theory-based finite element model [Lehtinen and Inan, 2008, 2009]. More recently, a large-scale computational model involving both the wave propagation and physical heating effects was developed to study the perturbation of ionosphere from a VLF transmitter [Graf et al., 2013]. A ray theory (wave hop)-based full-wave electromagnetic model that calculates the ionosphere reflection taking the concern of Fresnel diffraction was developed by Jacobson and Shao [2009; 2009]. With this model and observed LEMPs from Los Alamos Sferic Array, the reduction effects on electron density of the lower ionosphere from thunderstorms were revealed [Shao et al., 2006; Shao et al., 2012; Lay et al., 2014]. These results were based on the averaged lightning waveforms occurring in a small region within 5 min and a simplified inversion technique that matches the delay and amplitude of the peak of sky wave.

In this study, we present an improved EIWG model that can accurately simulate the propagation of a LEMP in EIWG through tracking all path effects of each independent ray of the LEMP, which is a growth of many previous works on ray theory and transfer matrix method for longwave propagation in the lower ionosphere [Wait, 1961; Berry et al., 1969; Nagano et al., 1975; Budden, 1988; Davies, 1990; ITURP, 2002; Nagano et al., 2003; Jacobson et al., 2009]. In the model, the lower ionosphere is assumed to be a magnetized, anisotropic, collisional, and cold vertical stratified plasma. The transfer matrix method [Price, 1964; Nagano et al., 1975; Nagano et al., 2003; Zhao et al., 2010] is applied to calculate the propagation property of each ray inside the dispersive ionosphere and therefore the reflection coefficient of each ray. Only the first- and second-order rays named first and second within the range of 1000 km are concerned, since the rays suffer higher attenuations through higher-order paths. The model is then applied to LEMPs recorded by a lightning detection network in central China [Qin, 2014; Qin et al., 2015]. Good matches between the modeled and observed results are achieved. Details of the model and its results are given in following sections.

2. Model Description

A lightning discharge can be treated as a spherically expanding EM wave source. A spherical EM wave in EIWG can be assumed as a summation of infinite plane waves in different directions, which is known as the angular spectrum decomposition. Each plane wave in a direction in time domain can be decomposed into the superimposition of cosine plane waves at different frequencies. For a source and a receiver at fixed positions, the dispersive effect in the ionosphere guides a different path for a different plane wave. The wave at each frequency always has a quasi-specular incident angle from the source to the receiver. So, one can first derive the transfer function for each plane wave at each frequency and its corresponding concentrated incident angle and then superimpose them into one to get the total waveform at the receiver. In other words, we can first calculate the amplitude and phase of the field of one beam of ray at one frequency along a specific path from a source. The total field at a receiver is then retrieved by integrating the field of all rays spanning all frequencies.

2.1. Parameterization of the Ionosphere

The lower ionosphere is set as a horizontally extended and vertically stratified, transitional, and collisional cold plasma region with a constant environmental Earth magnetic field. The wave packets of lightning source penetrate obliquely into the subionosphere. Although the ionosphere is bended we treat it as a horizontally extended one, as the size of ionosphere area interfering with the lightning wave is quite smaller than its sphere radius. For improving the accuracy in distant cases, the ionosphere focusing effect is accounted with a correction factor in subsequent calculations. The ionosphere is vertically parameterized into several homogeneous thin layers. The electron density profile (N_e) and electron-neutral collision rate (v_{en}) of the ionosphere are set as [Wait and Spies, 1964]

$$N_e = 1.43 \times 10^{13} \times e^{-0.15 \times z_0} \times e^{(\beta - 0.15) \times (z - z_0)} \quad (\text{m}^{-3}), \quad (1)$$

$$v_{en} = 1.8611 \times 10^{11} \times e^{-0.15 \times z} \quad (\text{s}^{-1}). \quad (2)$$

where β represents the sharpness and z_0 refers to the overall altitude of N_e . v_{en} is fixed in either daytime or nighttime. Only the effects of electrons are considered, as that of ions can be neglected in the lower ionosphere [Han and Cummer, 2010a].

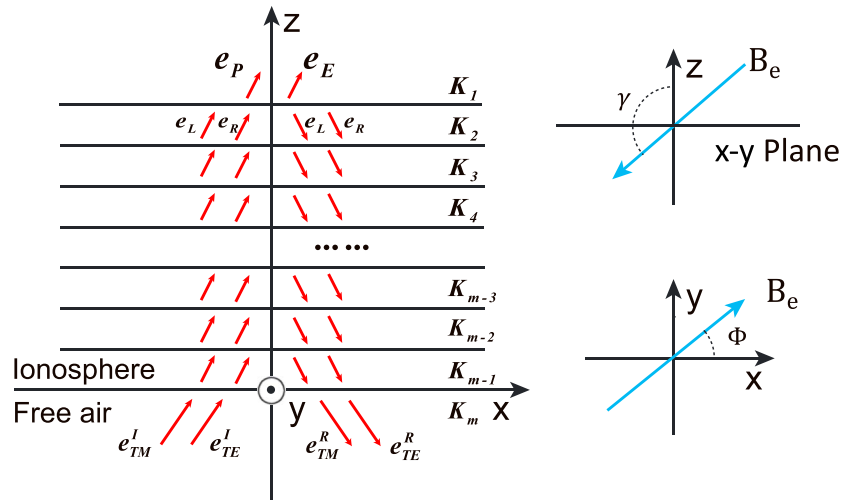


Figure 1. The geometry and coordinates for modeling of EM waves in the ionosphere based on transfer matrix method, with the indication of Earth magnetic field B_e .

Due to the Lorentz force produced by magnetic field and the damping effect by collisions, the lower ionosphere region is anisotropic and reflective to the VLF and LF waves. All these effects can be perceived in a susceptibility tensor matrix coupling in the numerical model of ionosphere in the next section [Budden, 1961].

2.2. Modeling of EM Waves in the Ionosphere

There are two basic numerical methods for solving the dispersion and reflection properties of electromagnetic field propagating in the horizontally stratified anisotropic lower ionosphere. The first one is the so-called full-wave method, which derives the Maxwell equations into a series of ordinary differential equation with respect to the ionosphere height z . With an initial solution at a sufficient height being provided, the whole field at any height is then obtained by numerical integrations [Clemmow and Heading, 1954; Budden, 1955; Pitteway, 1965; Jacobson et al., 2009]. The second one is the transfer matrix method, which divides the ionosphere into numerous discrete thin homogeneous layers. The field propagation effect in each layer is converted into a transfer matrix which involves the phase integration for each mode within the layer. The whole field at any height is then acquired by a series of matrix multiplication [Johler and Harper, 1962; Price, 1964; Inoue and Horowitz, 1966; Altman and Cory, 1969; Nagano et al., 1975; Nagano et al., 2003]. For the narrow- and high-frequency waves propagating in the ionosphere, the Wentzel-Kramers-Brillouin (WKB) approach is widely used [Budden, 1988]. Since the LEMP is lower frequency dominant, in this study we adopt the transfer matrix method [Nagano et al., 1975] to divide the ionosphere into many thin layers, the phase integration within each layer is based on the WKB solution and the four characteristic modes are coupled with each other at the boundary between any two layers. In the air below the ionosphere, we adopt the Ray Theory with the same incident angle finding technique used by Jacobson et al. [2009] and a modified transfer function to treat the LEMP propagation. The whole simulation is realized with the Matlab codes.

The geometry and coordinates for the ionosphere model are shown in Figure 1. The ionosphere is split into 700 layers from 40 km to 110 km with a thickness of 100 m (as shown in Table 1). According to Nagano et al. [1975], for the transfer matrix method a layer thickness of $\Delta Z = \lambda/2$ is corresponding to an error of 1%. As the field frequency in this study is capped at 150 kHz (as shown in Table 1), $\Delta Z = 100 \text{ m} = \lambda/20$ is enough for achieving a good accuracy. Each beam of ray of the lightning wave obliquely penetrates into the plasma region, with θ being the incident angle of the beam of ray from free air to the ionosphere and γ and Φ the angles of the Earth magnetic field to z and to x directions, respectively. The e_P and e_E at the top boundary stand for the “propagated wave” and “evanescent wave” there, respectively. In a given layer, Maxwell equations can be converted into the following form:

Table 1. Detailed Parameters Used for Modeling Lightning Sferics in the Region From 22°–41°N to 107°–127°E in Central China

Notation	Description	Value
Δf	Resolution of frequency decomposition	1 kHz
$\Delta\theta$	Resolution of incident angle span	0.25°
ΔZ	The thickness of layer in ionosphere model (vertical resolution of the ionosphere in the transfer matrix method)	100 m
$ \mathbf{B}_e $	Earth's magnetic field	$4.8 \times 10^{-5} \text{T}$
γ	Angle between \mathbf{B}_e and z axis	138°
Φ	Angle between \mathbf{B}_e and x axis in clockwise direction	0°, 90°, 180°, 270°
σ_e	Surface conductance of the Earth	0.005 S/m
ε_e	Relative dielectric constant of the Earth	15
Z_0	the overall altitude of N_e profile	$Z_0 = 70, \beta = 0.30$ for daytime,
β	the sharpness in N_e profile	$Z_0 = 84, \beta = 0.80$ for nighttime
h_i	The height from the Earth surface to the bottom of the subionosphere	40 km, top boundary is set to 110 km

$$\frac{d}{dz} \mathbf{e} = -jk_0 \mathbf{T} \mathbf{e}, \quad \mathbf{e} = \begin{bmatrix} E_x \\ -E_y \\ Z_0 H_x \\ Z_0 H_y \end{bmatrix}. \quad (3)$$

where \mathbf{T} is the coefficient matrix derived from Maxwell equations in each layer. \mathbf{T} and the wave number in z direction ($e^{jk_0 \sin(\theta) \Delta Z}$) form a transfer matrix \mathbf{K}_n in the layer n , which connects field vectors of its two boundaries as

$$\mathbf{e}_n = \mathbf{K}_n \mathbf{e}_{n-1}. \quad (4)$$

By applying boundary conditions at each interface, the field vector at each layer can be indicated as the function of field vectors by a group of multiplications from the top in downward direction if \mathbf{e}_P and \mathbf{e}_E at the top boundary are known (Figure 1). Due to that the only energy input into the ionosphere is the incident wave at the bottom of the ionosphere, it is reasonable to assume that only two upward waves remain at a relatively high altitude, which are known as “propagated wave” and “evanescent wave” [Budden, 1988]. These two waves at the top boundary of the model can be expressed as 2 eigenvectors of \mathbf{T} . Therefore, at the bottom of ionosphere, we have a boundary condition which connects the incident and reflected waves as

$$A \prod_{n=1}^{m-1} \mathbf{K}_n \mathbf{e}_P + B \prod_{n=1}^{m-1} \mathbf{K}_n \mathbf{e}_E = \mathbf{e}'_{TM} + \mathbf{e}'_{TE} + \mathbf{e}^R_{TM} + \mathbf{e}^R_{TE}. \quad (5)$$

with the A and B and E^R_{TM} and E^R_{TE} being figured out, fields at each layer can be retrieved recursively, and the reflection coefficients are given by

$$\begin{bmatrix} \parallel R_{\parallel} & \perp R_{\parallel} \\ \parallel R_{\perp} & \perp R_{\perp} \end{bmatrix} = \begin{bmatrix} \frac{E^R_{TM}}{E^I_{TM}} & \frac{E^R_{TE}}{E^I_{TM}} \\ \frac{E^R_{TM}}{E^I_{TE}} & \frac{E^R_{TE}}{E^I_{TE}} \end{bmatrix}. \quad (6)$$

It should be mentioned that the reflection coefficients here represent for the phase shifting in z direction, since the component $e^{jk_0 \cos(\theta)x}$ is omitted to simplify the calculation as well as the $e^{j\omega t}$.

2.3. Derivation of the Transfer Functions

In ray theory, EM fields at receiver are retrieved by superimposition of numbers of discrete rays through different paths which are reflected by the ionosphere one or more times [Wait, 1961; Berry et al., 1969; Davies, 1990].

We restrict our model range to be less than 1000 km, which is far from the caustics distance ($2\sqrt{2R_e h_s}$, 1750 km for $h_s = 60$ km) of EIWG to avoid the effect of diffraction for simplification [Wait, 1961]. The geometry and coordinates for EIWG model based on ray theory are shown in Figure 2. The source at ground is the

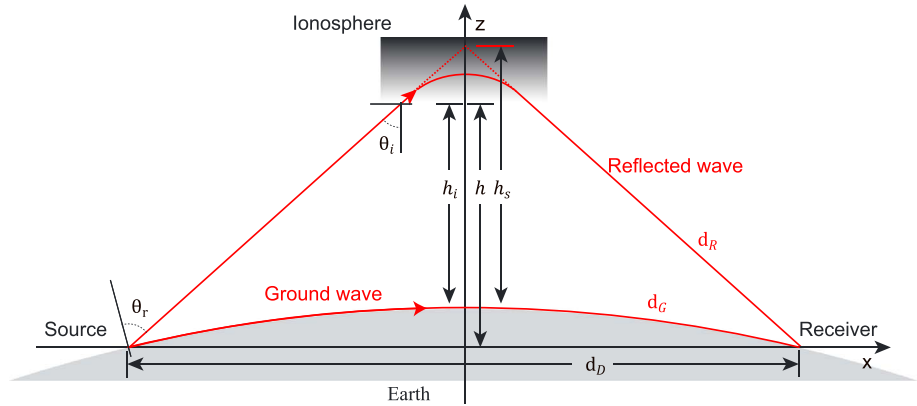


Figure 2. The geometry and coordinates for EIWG model based on ray theory. There are several paths from the source to receiver, only the most significant two are shown, the ground wave and first hop of the reflected wave.

lightning discharge, which emits EM waves in a spherical expansion manner. Most contributions to the receiver are raypaths laid in the plane containing the source and receiver and vertical to ground, which are chosen for calculations.

The transfer function is defined and derived based on the propagation effect combining with the amplitude factor according to classical ray theory [Wait, 1961; Berry et al., 1969; ITURP, 2002; Pal, 2015].

The phase integration along whole path including the unknown part inside the ionosphere in x direction is well represented by $e^{-jk_0 \sin(\theta_i)d_D}$, as well as $_{\parallel}R_{\parallel} e^{-jk_0 2 \cos(\theta_i)h}$ for z direction. Since a lightning discharge is a vertical dipole as a whole, its radiated waves are dominated by traverse magnetic (TM) mode. As the receiver is set close to the ground, only the vertical E field is of concern. For a vertical antenna, the vertical E field at ground of first hop is given by

$$E_1(\omega) = \frac{2E_0(\omega) [\sin(\theta_r)]^2 {}_{\parallel}R_{\parallel} F_i F_t F_r e^{-jk_0 [\sin(\theta_i)d_D + 2 \cos(\theta_i)h]}}{d_R} \tag{7}$$

where h is the height from bottom of the ionosphere to the horizontal line connecting the source and receiver, d_G the distance of ground wave path, θ_i the concentrated incident angle, d_R the total distance of reflecting path, d_D the direct distance from source to receiver, h the height from original point to bottom of the ionosphere, and θ_r the angle between the incident ray to the normal of Earth at source point. Once d_G , $_{\parallel}R_{\parallel}$, and ω of E_0 are determined, θ_i can be retrieved by a phase unwrapping process suggested by Jacobson et al. [2009]. The phase swapping process is to find the angle that has the maximum phase integration among all incident angles, which is also known as the quasi-specular incident angle or the concentrated incident angle in this study. Assuming that the wave number k_x ($k_0 \sin(\theta_i)$) or the phase velocity in x direction never changes in each part of the model, d_R is then given by $d_D/\sin(\theta_i)$.

Since we treat the ionosphere as a horizontal interface, a focusing factor F_i (an amplitude correction parameter) is introduced to correct the focusing effect of curvature of the ionosphere. F_i can be estimated from geometrical optics [Wait, 1961; ITURP, 2002], and this estimate is only valid in lightning area ($d_G < 2\sqrt{2R_E h_s}$) of the wave propagation. Here R_E is the Earth radius and the quasi-specular reflection height h_s is derived from d_R and d_D .

$$F_i = \frac{R_E + h_s}{R_E} \left[\frac{2 \sin(\frac{\theta_i}{2})}{\sin(\theta_i)} \right]^{\frac{1}{2}} \cdot \left[\frac{R_E + h_s - R_E \cos(\frac{\theta_i}{2})}{(R_E + h_s) \cos(\frac{\theta_i}{2}) - R_E} \right]^{\frac{1}{2}} \tag{8}$$

Although h_s and F_i are estimates, they make the model achieve a high accuracy as will be seen from the modeling results in section 4. The F_t and F_r are the antenna factors which only start taking effect when the ground distance is farther than 1500 km at a 60 km reflection height. Assuming them equal to 1 will always be valid at a shorter distance (<1000 km). Similarly, the transfer function of vertical E field of second hop is

$$E_2(\omega) = \frac{2E_0(\omega) [\sin(\theta_i)]^2 ({}_{\parallel}R) F_i F_t F_r e^{-jk_0 [\sin(\theta_i)d_D + \cos(\theta_i)(2h+2h_i)]}}{d_R} \tag{9}$$

This transfer function indicates that there are no pure TM waves existing in the ionosphere. The reflected field $E_2(\omega)$ includes both the TM and traverse electric (TE) waves induced by the ionosphere during the first reflection process. In equation (9), the ground is assumed to be uniform with a finite conductance σ_e and a dielectric constant ϵ_e , resulting in $R_{G\perp} = R_{G\parallel} = \frac{\cos(\theta) - \Delta_g}{\cos(\theta) + \Delta_g}$, $\Delta_g = \frac{k_0}{k_e} \sqrt{1 - \frac{k_0^2}{k_e^2} \sin^2(\theta)}$ for VLF/LF waves for both TM and TE modes. In general, the $R_G \approx 1$.

The transfer function of the ground wave is calculated by Fock's diffraction equation [Fock, 1965], which takes the summation of a few number of discrete mode acquired by solving the mode equations [Shao and Jacobson, 2009]:

$$E_G(\omega) = \frac{E_0(\omega)W(\omega)e^{-jk_0d_G}}{d_G}, \quad (10)$$

$$W(\omega) = 2e^{-j\frac{\pi}{4}} \sqrt{\pi X(\omega)} \sum_{s=1}^{\infty} \frac{e^{-j\pi t_s(\omega)}}{t_s(\omega) - q(\omega)^2}. \quad (11)$$

Same to equation (9), the Earth surface is assumed to be uniform with a finite conductance σ_e and a dielectric constant ϵ_e . The source and receiver both are supposed to be on ground.

The lightning discharge is assumed to be a point dipole without spatial structure. In general, the most intense radiation field of a lightning stroke comes from the lower part of the lightning channel. And the size of this part of channel comparing to the EIWG propagation geometry is small enough to be regarded as a point source. Heidler's notation is adopted to express the current waveform of the point dipole. Below is the current adopted for simulations in section 3, where $\tau_1 = 10 \mu\text{s}$, $\tau_2 = 45 \mu\text{s}$, and $n = 2$:

$$I(t) = \frac{I_0}{\eta} \frac{(t/\tau_1)^n}{[(t/\tau_1)^n + 1]} e^{-t/\tau_2}, \quad \eta = \exp\left(-\frac{\tau_1}{\tau_2} \left(n \frac{\tau_2}{\tau_1}\right)^{1/n}\right). \quad (12)$$

The input field $E_0(t)$ from the point-dipole source is given by

$$E_0(t) = \frac{L_0}{4\pi\epsilon_0 c^2} \frac{dI}{dt}, \quad E_0(\omega) = \int_{-\infty}^{\infty} E_0(t) e^{-j\omega t} dt. \quad (13)$$

The angular factor $\sin(\theta_i)$ for a dipole radiation is not included in equation (13) but is included in equations (7) and (9). The total field at the receiver is then given by

$$E(t) = \int_{-\infty}^{\infty} \left(E_G(\omega) + \sum_{i=1}^{\infty} E_i(\omega) \right) e^{j\omega t} d\omega. \quad (14)$$

Only the first hop is considered in subsequent model analysis, since sky waves nearer than 1000 km are dominated by the first hop, and spatial inhomogeneous of the ionosphere may introduce inaccuracy on the second hop.

3. Modeling Results for General Cases

To examine the model, we have simulated the lightning sferics under general conditions during day and night times with it. The region chosen for simulation is from 22° – 41°N to 107° – 127°E in central China, where we have a lightning sferic detection network (shown in section 4) installed.

There are three main physical parameters that dominate the pattern of lightning sky wave in the model: ionosphere electron density (N_e), electron-neutral collision rate (ν_{en}), and Earth magnetic field (\mathbf{B}_e). For daytime and nighttime in the chosen region, ν_{en} profile is assumed to be stable and does not vary with location and time (see equation (2)) [Wait and Spies, 1964], \mathbf{B}_e vector is from the International Geomagnetic Reference Field website [Thébault et al., 2015], Z_0 and β of N_e profile are obtained by fitting equation (1) to the averaged local electron distribution of July 2012 from the International Reference Ionosphere (IRI) model [Bilitza et al., 2011], only in the range of 10^6 – 10^9 as reference, as shown in Figure 3. The exponential profile is capped at 10^9 m^{-3} since those regions with higher N_e would not interact with waves at frequencies lower than 150 kHz.

The ground conductance and dielectric constant for the simulation for the chosen region are following the recommendations of International Radio Consultative Committee (CCIR) [ITU-RP, 1999]. The lightning source

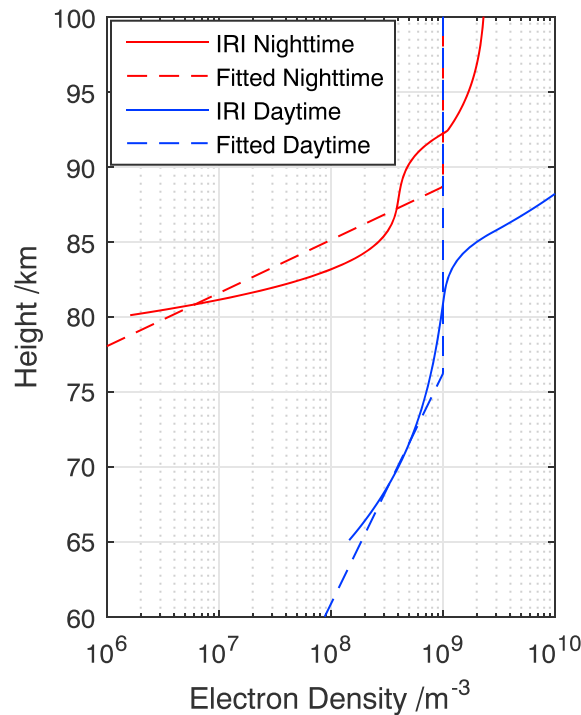


Figure 3. The adopted daytime and nighttime ionosphere electron density profiles (dashed lines) for the simulation in section 3. They are determined by fitting the Wait and Spies model (equation (1)) to IRI model (solid lines) only in the range $10^6 \sim 10^9 \text{ m}^{-3}$.

at high frequencies than in daytime, resulting in a sharper sky wave in nighttime than in daytime. This means that a VLF/LF pulse is attenuated more through EIWG in daytime than in nighttime.

Above spheric features can be attributed to the difference in electron density of the ionosphere during daytime and nighttime. The ionization of ionosphere *D* region is induced by the Lyman series-alpha hydrogen radiation (wavelength = 121.5 nm) ionizing the nitric oxide (NO) and the hard X-ray (wavelength < 1 nm) ionizing the N_2 and O_2 , with solar activities as the main radiation source in daytime and the cosmic rays maintaining it at night [Pavlov, 2013]. The electron density profile becomes sharper and shrinks to a higher height at night when the radiation decreases. Since the higher region has a lower neutral particle density, a lower electron-neutral particle collision rate and less attenuation effect on the EM field accelerate electrons there. Besides, a sharper ionosphere transition region at night also shortens the penetration depth of waves, making the attenuation decrease. As a result, the ionosphere at night has relatively lower absorbing rate than in daytime.

Shown in Figure 5 are the simulation results similar to Figure 4, but for a fixed source-receiver distance of 500 km with different wave propagation directions. It can be seen that the angle of the wave propagation direction to the Earth magnetic field has significant influences on the sky waves at night. During daytime, the sky wave is more regular and almost the same for different wave propagation directions. The difference in the Earth magnetic field only slightly changes the sky wave amplitude. During the nighttime, the spheric waveform is more complicated. For $\Phi = 0^\circ/180^\circ$, the spheric waveform has no more difference from that of daytime except longer time delays. For $\Phi = 90^\circ$, there is an enhancing effect below 40 kHz and around 80 kHz, resulting in a notable increase in amplitude of the spheric waveform. Particularly, for $\Phi = 270^\circ$ the sky wave of the spheric tends to have double peaks rather than a single peak with enhancements existing around 50 kHz and 120 kHz. Moreover, it is worth to mention that the direction of Earth magnetic field also has a big influence on the amplitude of sky wave during nighttime. When Φ is around $0^\circ, 180^\circ$, or 270° , the amplitude of the sky wave is supposed to be slightly lower than that of the ground wave, as shown in Figures 4c and 5c. But when Φ lies in the vicinity of 270° , the first hop reflection is separated into two pulses, leading to a decrease in its amplitude.

current is based on equation (12), which has a rise time of $10 \mu\text{s}$ and fall time of $45 \mu\text{s}$. Details of the parameters used in the simulation and their descriptions are given in Table 1. The simulation is implemented in frequency bands from 3 kHz to 150 kHz, due to the incoherence of lower ionosphere to higher-frequency waves and the invalidation of ray theory at lower frequencies. E_0 is filtered (3 kHz–150 kHz band pass) before inputting into the model to avoid some oscillations produced by cutoff effect in frequency domain.

Shown in Figure 4 are the simulated lightning-induced ground waves and sky waves for daytime and nighttime at different ground distances with $\Phi = 0^\circ$ (the wave propagates from north to south). The results show that the lower ionosphere (*D/E* region) has a strong low-pass feature and a significant absorbing effect to high frequencies. When the distance goes farther the ratio of sky wave to ground wave increases. The ionosphere in nighttime has a relatively higher reflection rate

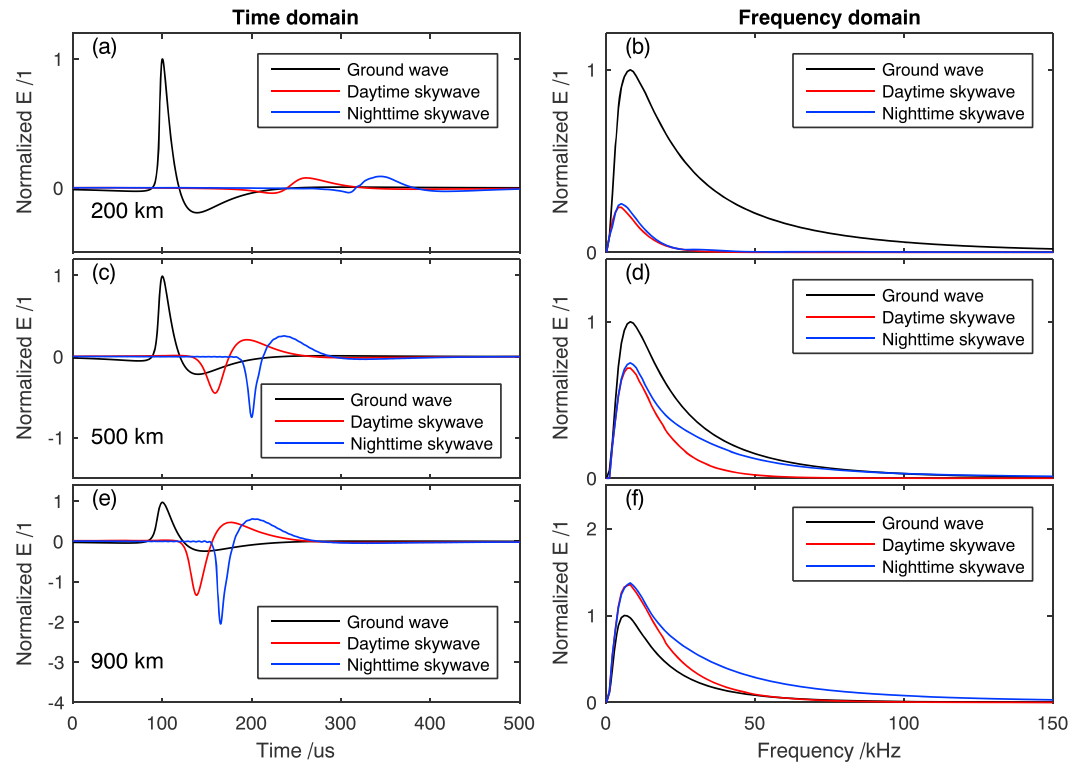


Figure 4. Modeling results of lightning-induced ground waves and spherics for (a, c, e) daytime and (b, d, f) nighttime at different distances (200 km, 500 km, and 900 km, respectively) for $\Phi = 0^\circ$ (the wave propagates from south to north) for the region of $22^\circ\text{--}41^\circ\text{N}$ to $107^\circ\text{--}127^\circ\text{E}$ in central China, in both time and frequency domains. Other parameters are listed in Table 1.

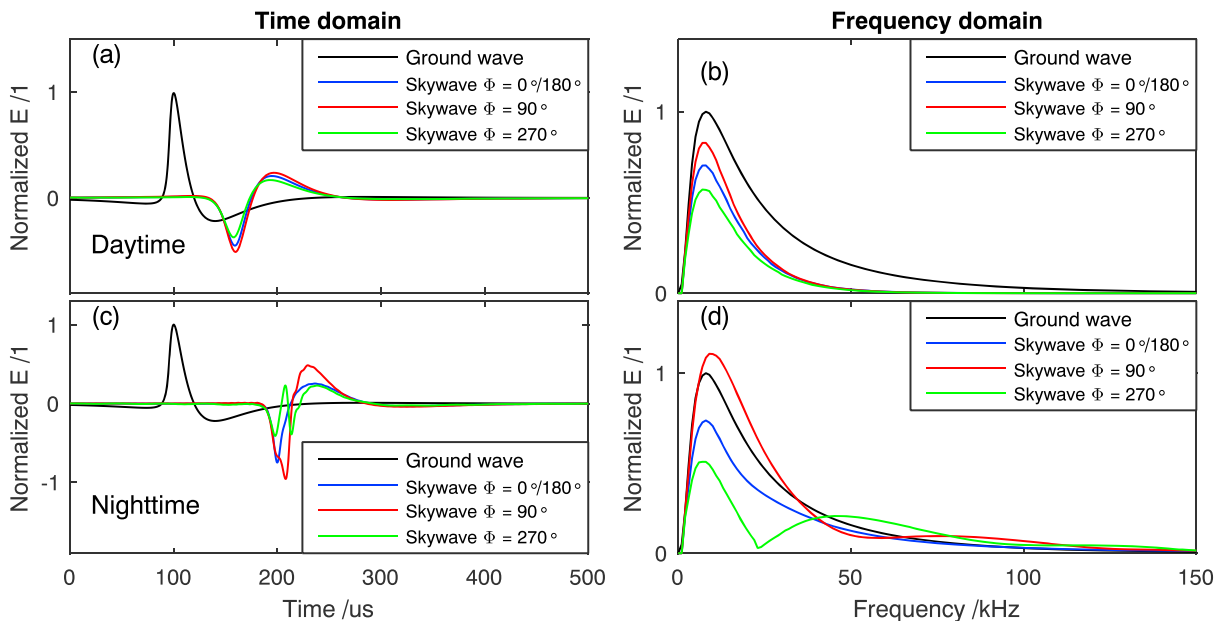


Figure 5. Similar to Figure 4 but for a fixed source-receiver distance of 500 km with different wave propagation directions: $\Phi = 0^\circ$ (north to south), 90° (west to east), 180° (south to north), and 270° (east to west). Other parameters are listed in Table 1.

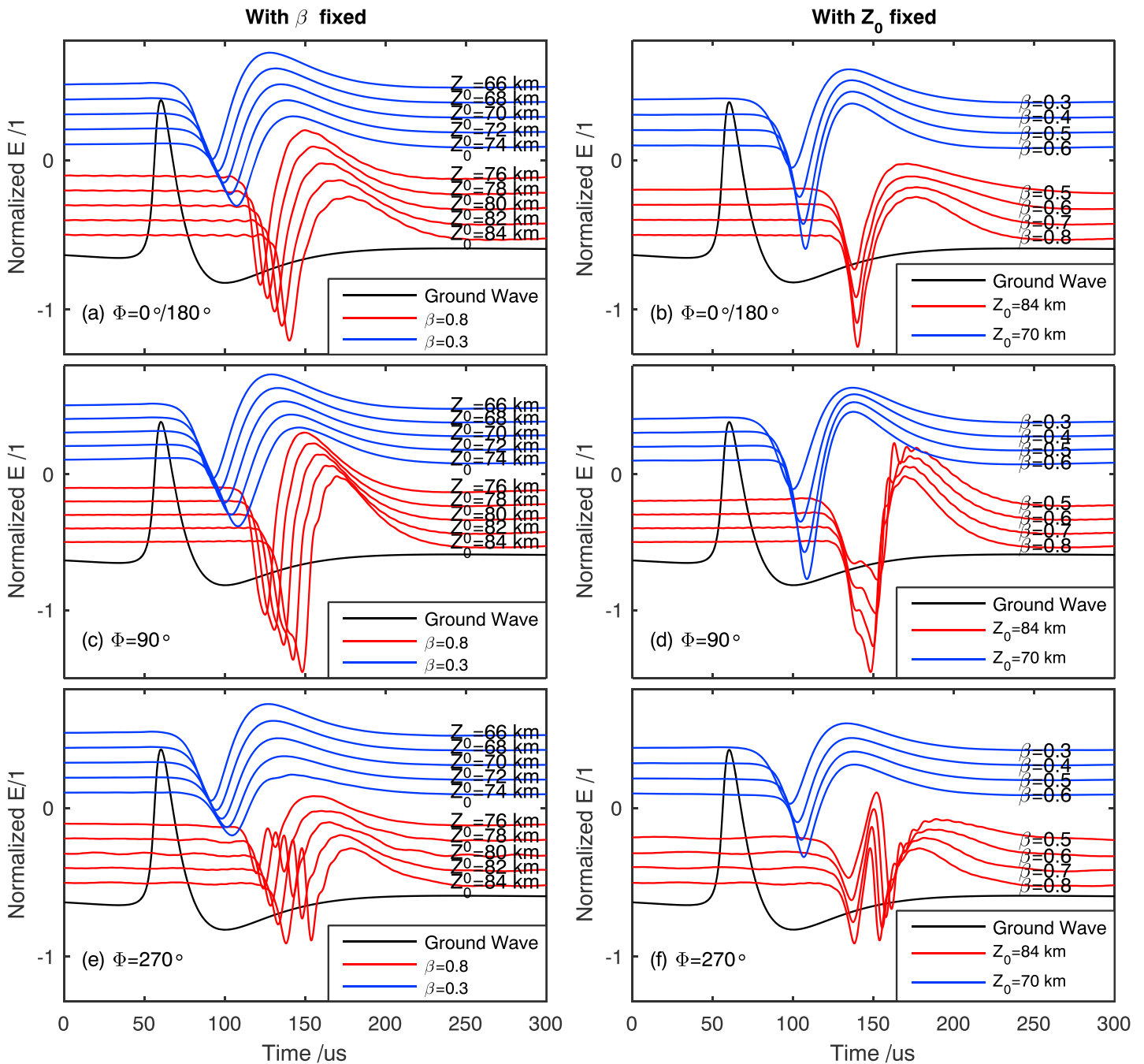


Figure 6. A comparison of the sky wave patterns simulated with different ionosphere electron density profiles at a fixed distance of 500 km. (a, c, e) For β fixed to 0.3/0.8 and Z_0 changing from 66 to 84 km. (b, d, f) For Z_0 fixed to 70/84 km and β changing from 0.3 to 0.8, for $\Phi = 0^\circ/180^\circ, 90^\circ,$ and $270^\circ,$ respectively.

Jacobson *et al.* [2012] reported that during the nighttime an eastward propagating radio wave below 30 kHz would be enhanced and a westward one beyond 50 kHz would be enhanced, which is a little bit different from the present results probably due to the different regions studied. They also reported that a westward radio wave would have a complicated or multiple-peaked pattern of first hop sky wave during nighttime. The double-peak sky wave (dispersed sky wave) in lightning sferics (as shown in Figure 5c, green line) has been reported before by Lay and Shao [2011a] too, but with no reasonable explanations. Based on the modeling results in this section and observation results in next section, we suggest that both the enhancement and the double-peak phenomena of the lightning sky wave during nighttime may be attributed to

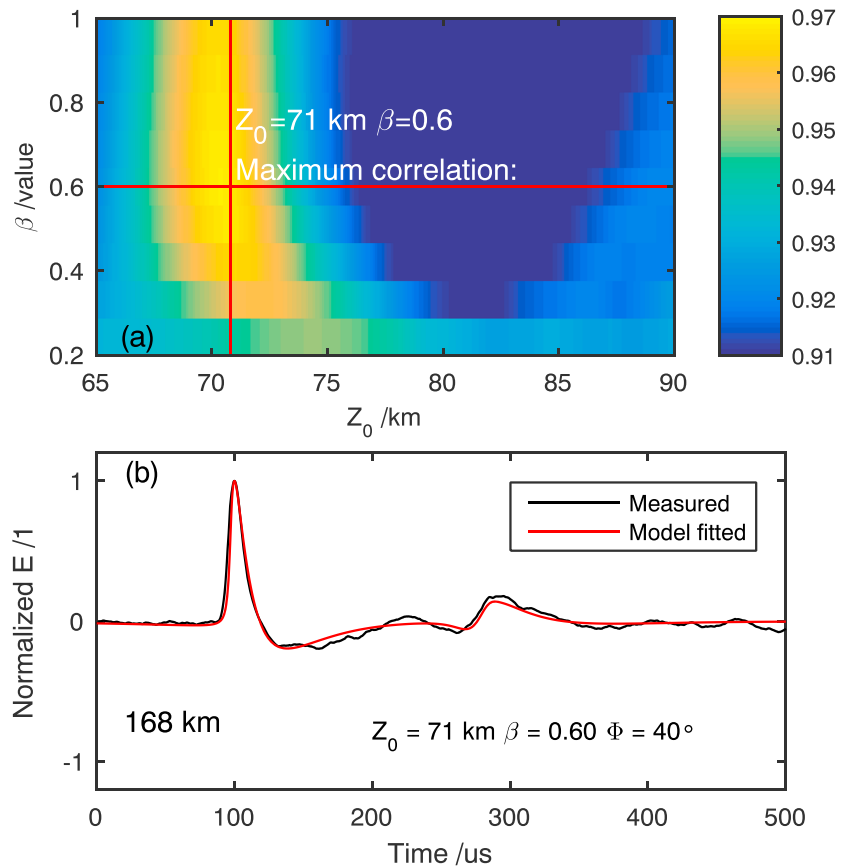


Figure 7. An example for illustration of the process of curve fitting of a measured lightning sferic with the model: (a) the correlation coefficient map for the measured lightning sferic (black line in (b)), for a Z_0 span of 65–90 km and a β span of 0.2 to 1.0, with given source and receiver locations and B_e . The maximum correlation coefficient occurs at $Z_0 = 71$ km and $\beta = 0.6$, and the best curve fitting is shown in red in Figure 7b.

the magneto-ionic splitting of LEMP in the D/E region due to the Earth magnetic field. Detailed interpretation is given in the next section following Figures 8 and 9.

Shown in Figure 6 is a comparison of the first hop sky waves simulated with different ionosphere electron density profiles at a fixed distance of 500 km, for sensitivity testing of the ionosphere profile versus the sky wave. Apart from the obvious difference between events with different propagation direction, the sky wave waveform slightly changes with the variation of Z_0 and β . The Z_0 value mainly affects the delay of the sky wave to ground wave, and the β value changes the sharpness of the first hop sky wave. Such difference in sky wave pattern between different ionosphere profiles makes it practicable to retrieve the actual electron density distribution of ionosphere by curve fitting the observed lightning sky wave with the model. In the next section, a curve fitting of lightning sferic technique is introduced and practiced to retrieve the electron density profile of lower ionosphere, for various lightning sferics measured in daytime and nighttime.

4. Modeling Results for Measured Lightning Sferics

During the summer of 2012, we built a local lightning detection network in the region of 22° – 41° N to 107° – 127° E in central China [Qin, 2014; Qin et al., 2015]. The receiver at each station consists of a monopole vertical antenna with an 800 Hz–450 kHz preamp circuit, a continuously recording system with a sampling rate of 5 MHz at 12 bits and a GPS system with a timing deviation of 50 ns per month, resulting in a time accuracy of 0.2 μ s. The receiver is designed for sensing a 100 kA stroke at a distance of 100 km at its full range. Since its setup a great number of lightning sferics within 1000 km have been recorded with the network. Some of these lightning sferics are chosen for investigation with the present model. It should be mentioned

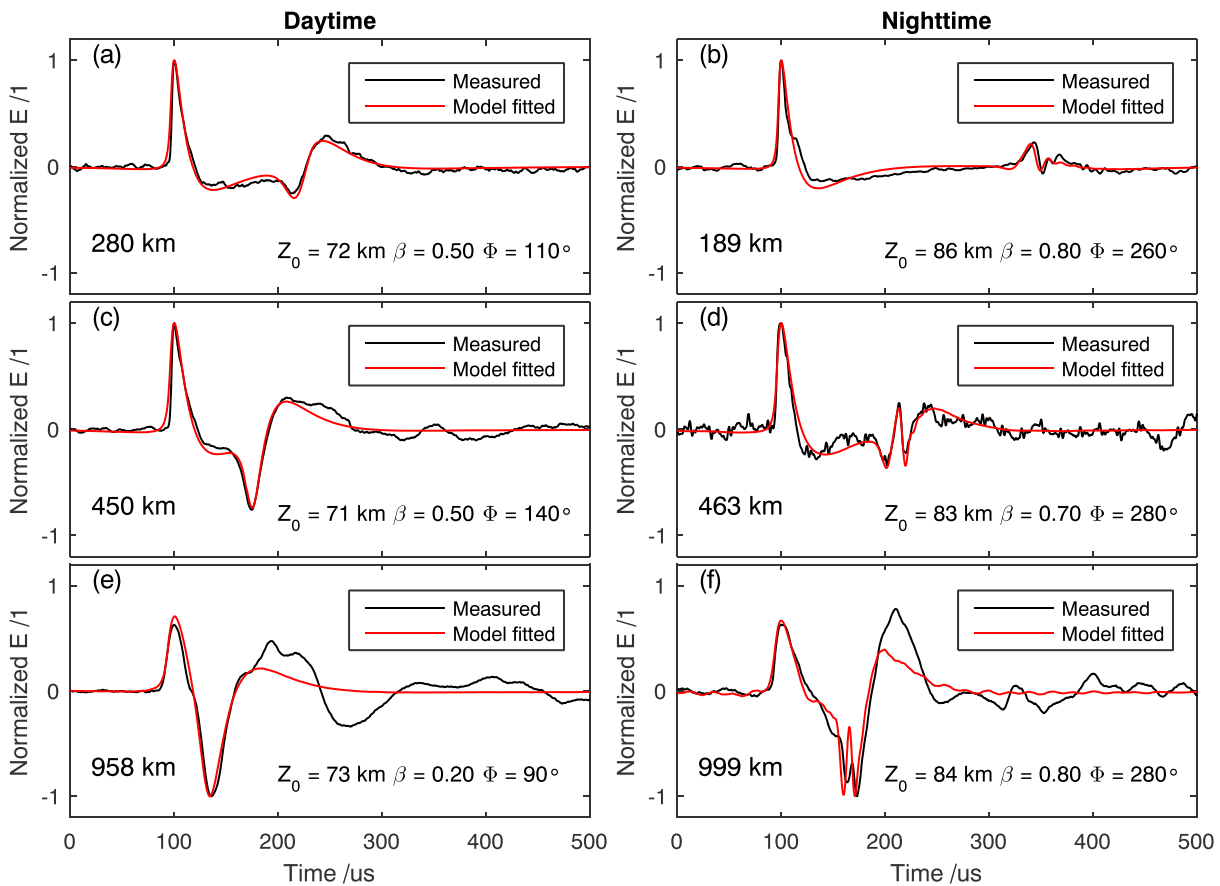


Figure 8. Model fitting results for lightning return stroke sferics measured with a VLF/LF lightning detection network in central China. Return strokes in daytime in ranges of (a) 280 km, (c) 450 km, and (e) 958 km. Return strokes in nighttime in ranges of (b) 189 km, (d) 463 km, and (f) 999 km. The Earth magnetic field is set according to the source and receiver locations of each return stroke sferic. The best model fitting is found by tuning the ionosphere electron density profile in the range of β : 0.1–1.0 and Z_0 : 65–90 km.

that different frequency bandwidth of a receiver may lead to different measured waveform of a lightning sky wave. For example, the waveform in Figure 8a of this paper is different to Figure 2f of Haddad et al. [2012] which was measured with a Fast Antenna having a bandwidth from several ten hertz to several megahertz. The relatively higher lower cutoff frequency of the receiver makes the measured waveform in this paper lack of some ELF components. Since the model in this paper is only suitable for waves with frequencies higher than 3 kHz, the receiver bandwidth will not affect the model application.

For a measured lightning sferic with given source and receiver locations, the propagation paths of its ground wave and sky wave are known, and the Earth magnetic field (B_e and Φ) corresponding to the sky wave reflection area is predetermined. The lightning source input electric field (E_0) is acquired by first cutting down the ground wave part (E_G) from the measured sferic waveform and then transform the E_G back by an inversed ground wave transfer function as

$$E_0(\omega) = E_G(\omega) * \left(\frac{W(\omega)e^{-jk_0d_G}}{d_G} \right)^{-1}. \quad (15)$$

With the acquired E_0 as the input, the sferics (ground plus sky waves) at the receiver for all possible ionosphere electron density profiles (N_e : β and Z_0) are calculated with the model to build a library. A correlation coefficient map is then made by comparing the measured sferic to each calculated sferic in the library. The one having the maximum correlation coefficient (leading to the best fitting of the measured lightning sferic) is considered as the most accurate model prediction, and the corresponding β and Z_0 inputs are considered as the ionosphere electron density profile for the concerned sky wave reflection area.

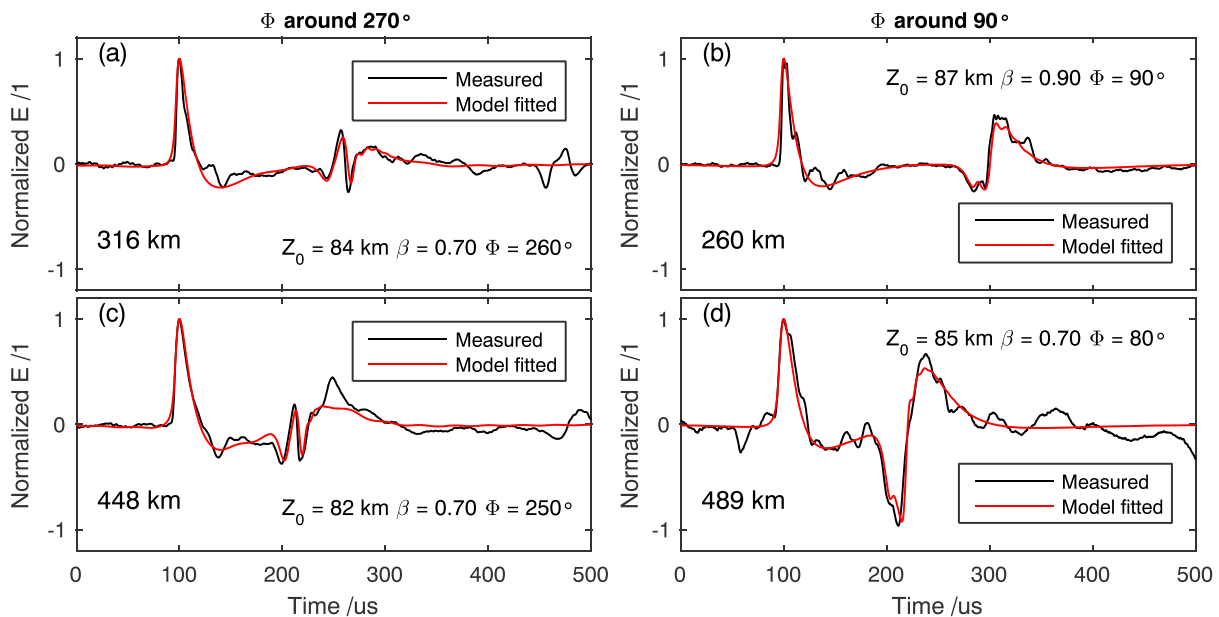


Figure 9. Similar to Figure 5 but focused on lightning sferics with a double-peak (dispersed) sky wave pattern observed in nighttime. Events, which are in ranges of (a) 316 km and (c) 448 km and with Φ around 270° , show obvious double-peak patterns. Events, which are in ranges of (b) 260 km and (d) 489 km with Φ around 90° , only have a slight oscillation but a significant enhancement in amplitude at their sky wave peaks.

Comparing to previous inversion techniques of the electron density profile of lower ionosphere, Thomson derived the profile with the received amplitude and phase from narrowband long radio waves [Thomson, 2004, 2005; Thomson et al., 2007; Thomson, 2010]; The Duke Group fitted the profile according to frequency domain features [Cheng and Cummer, 2005; Cheng et al., 2006; Han and Cummer, 2010a, 2010b; Han et al., 2011]; Shao and Jacobson retrieved the profile by matching the time delay and amplitude of one inversed sky wave peak in modeling output with the observed waveform [Shao et al., 2012; Lay et al., 2014]. The present work directly utilizes the curve fitting of the observed sky wave waveform in time domain to inverse the ionosphere electron density profile. Shown in Figure 7 is an example for illustration of above stated curve fitting process, where (a) is the correlation coefficient map for the measured lightning sferic (black line) in (b), for a Z_0 span of 65 to 90 km and a β span of 0.2 to 1.0, with given source and receiver locations and B_e . The maximum correlation coefficient occurs at $Z_0 = 71$ km and $\beta = 0.6$. The best curve fitting is shown in red (Figure 7b). The same curve fitting technique is then applied to several sferics measured at daytime and nighttime at different distances and their results are shown below in Figures 8–10.

Shown in Figure 8 are the model fitting results for several lightning return stroke sferics measured with the network in central China. Figures 8a, 8c, and 8e are for three LEMPs in daytime, and Figures 8b, 8d, and 8f are for three LEMPs in nighttime. It can be seen that the measured waveforms match reasonably well with the model fittings. Particularly, the sky waves in nighttime show more complicated patterns than those in daytime, as predicted with the model in section 3 above. The fitting results in Figures 8e and 8f have some mismatches after the first hop peak. This is due to that the second hop and subsequent hops might be superimposed on the first hop when the distance is farther than 800 km, but the model just takes account the first hop.

Figure 9 is similar to Figure 8, but is focused on lightning sferics with a double-peak reflection (dispersed sky wave) measured during nighttime. It should be particularly mentioned that both our simulations in section 3 and observations in this section show that a nighttime sferic only with a Φ around 270° usually has such a pattern, as shown in Figures 8d and 8f and 9a and 9c, while the one with a Φ around 90° only has a slight oscillation around its peak, as shown in Figures 9b and 9d. A nighttime sferic with a Φ around 0° or 180° usually is similar to a daytime one, i.e., has only one inversed peak in its waveform.

Based on the modeling results in the previous section and the observed results in this section, we suggest that the double-peak sky wave in nighttime might be a result of magneto-ionic splitting effect in the lower

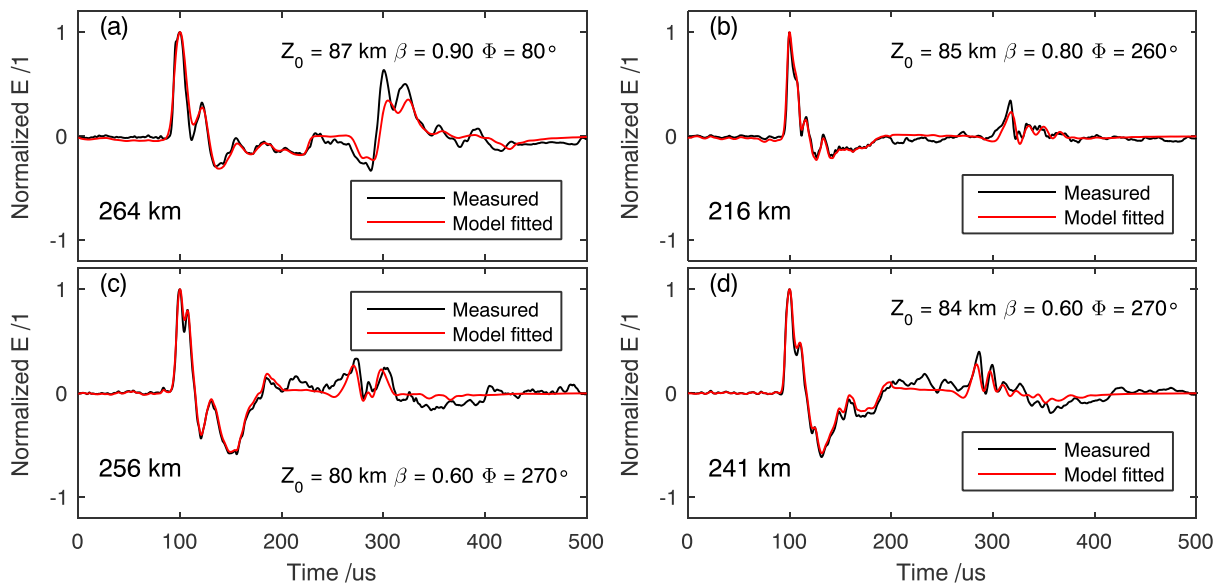


Figure 10. Similar to Figure 8 but for some events with much more complicated sferic waveforms like the first return strokes during nighttime.

ionosphere due to the Earth magnetic field [Budden, 1988]. The Earth magnetic field splits the LEMP into two characteristic mode wave packets as it propagates within the ionosphere. For a westward LEMP in nighttime (Φ around 270° , as shown in Figures 8d and 8f and 9a and 9c), the Earth magnetic field makes the two characteristic modes significantly different in their phase propagation paths, thus a double-peaked pattern of sky wave is formed. For a LEMP propagating at an inverse direction (Φ around 90° , as shown in Figures 9b and 9d and 6c and 6d), the Earth magnetic field makes the two characteristic modes no more different in their phase propagation paths, resulting in a single peaked but enhanced and wider pattern of sky wave. Further analysis of this phenomenon will be our next work.

Shown in Figure 10 are the results for events with much more complicated sferic waveforms like first return strokes during nighttime. Although these cases are no more than 300 km in distance, the ground wave can be split easily from the sky wave due to the relatively large time delay between them at this distance.

All above results indicate that the present model can serve as an effective tool for long-term monitoring of lower ionosphere in good temporal and spatial resolutions with a lightning sferic detection network.

5. Summary and Discussion

An improved ray theory and transfer matrix method-based model for simulation of a LEMP propagating in the EIWG is proposed. The model includes the representation of lightning source, parameterization of the ionosphere, establishment of the transfer function representing all effects of the ionosphere on the LEMP, and determination of the attenuation mode of ground wave of the LEMP. The lightning source is treated as an electric point-dipole standing on ground. The transfer function for the sky wave is established based on ray theory and transfer matrix method. The attenuation mode of the ground wave is solved from mode equations. With given ionosphere parameters, the model is able to predict the lightning sferic reflected from the ionosphere. With a given lightning sferic, the model is able to retrieve the properties of the ionosphere. The model is adequate for lightning sferics in ranges within 1000 km and in VLF/LF bands.

To test the model, we have simulated the lightning-induced ground and sky waves under general conditions for both daytime and nighttime. The results show that the ionosphere has a strong low-pass feature and significant absorbing effect to high frequencies. The ionosphere in nighttime has a relatively higher reflection rate at high frequencies than daytime. In daytime, the lightning sky wave shape is regular and similar for different wave propagation directions. But at night, the sky wave shape is more complicated and changes with the wave propagation direction.

The model has also been applied to 14 lightning return stroke sferics measured in both daytime and nighttime in ranges of 200–1000 km. By using the ground wave as the input, all the measured sferics, either simple or complicated waveforms, are well fitted with the model through tuning the ionosphere electron density profile. It should be noted that both our simulations and observations show that the lightning sferic waveform in nighttime is more complicated than in daytime. Particularly, when a LEMP propagates from east to west at night, its sky wave waveform tends to be a double peak (dispersed) one rather than a single peak. While most previous studies often treated the sky wave of lightning sferic with only one inversed peak [Lay and Shao, 2011b; Shao et al., 2012; Lay et al., 2014], we speculate that the double-peaked (dispersed) sky wave in westward lightning sferic in night and the enhanced sky wave in eastward lightning sferics in night may be caused by the magneto-ionic splitting effect of Earth magnetic field on LEMP in cold plasma in the lower ionosphere. More detailed analysis of this phenomenon is going to be implemented in our future work.

The model performs a high resemblance to lightning sferics in both daytime and nighttime under different ionosphere conditions. It provides us an efficient way to retrieve the distribution of electron density of the ionosphere and hence to monitor the change of the ionosphere with LEMPs. Furthermore, the two parameters, Earth magnetic field and collision rate of electron-neutral particle in the ionosphere, are found to have significant influences on the pattern of lightning sferics. The double-peak (dispersed) sky wave events at night are particularly sensitive to these two parameters. With this finding, the model may be applied for detecting the anomalous variation of the geomagnetic field and neutral particle precipitation in the ionosphere with lightning sferics.

Comparing to the present model, the mode theory-based model [Cummer et al., 1998; Cheng et al., 2006; Marshall and Inan, 2010] has a limit that it relies on the top boundary to be consistent along the whole path, which may lead to the unknown inaccuracies caused by the natural spatial inhomogeneity of the ionosphere. The present model only depends on the state of the ionosphere at the reflection point, thus making it a suitable tool to monitor the ionosphere in a higher time and space resolution with lightning sferics. Although the FDTD model [Hu and Cummer, 2006; Marshall, 2012] is a powerful tool with great precision, burdensome computing makes it almost impossible to solve the inversion problem especially under situations that the parameter library is huge. The Jacobson's full-wave model [Jacobson et al., 2009; Shao et al., 2012; Lay et al., 2014] is also an efficient tool to probe the ionosphere, but their technique retrieving the ionosphere electron density profile could be further improved. They retrieved the ionosphere electron density profile by matching the time delay and amplitude of the inversed sky wave peak modeled with that observed [Shao et al., 2012; Lay et al., 2014], which may cause ambiguity when applying to the double-peaked sky wave in nighttime. While in the present work we directly use the curve fitting of the observed sky wave waveform with the modeling result to inverse the ionosphere electron density profile.

Acknowledgments

Works leading to this paper are funded by the Hong Kong Polytechnic University, Research Grant Council of Hong Kong Government (grant PolyU5123/13E), and National Natural Science Foundation of China (grants 41374160 and 41075001). Authors would like to thank Zhao Shufan for the discussion on transfer matrix method.

References

- Altman, C., and H. Cory (1969), The generalized thin-film optical method in electromagnetic wave propagation, *Radio Sci.*, *4*, 459–470, doi:10.1029/RS004i005p00459.
- Berry, L. A., G. Gonzalez, and J. L. Lloyd (1969), Wave-hop series for an anisotropic ionosphere, *Radio Sci.*, *4*, 1025–1027, doi:10.1029/RS004i011p01025.
- Billitz, D., L.-A. McKinnell, B. Reinisch, and T. Fuller-Rowell (2011), The international reference ionosphere today and in the future, *J. Geodesy*, *85*(12), 909–920.
- Budden, K. G. (1955), The numerical solution of the differential equations governing the reflexion of long radio waves from the ionosphere. II, *Philos. Trans. R. Soc. A*, *248*(939), 45–72, doi:10.1098/rsta.1955.0009.
- Budden, K. G. (1961), *The wave-guide mode theory of wave propagation*, Logos Press, London.
- Budden, K. G. (1988), *The Propagation of Radio Waves: The Theory of Radio Waves of Low Power in the Ionosphere and Magnetosphere*, Cambridge Univ. Press, Cambridge, UK.
- Cheng, Z., and S. A. Cummer (2005), Broadband VLF measurements of lightning-induced ionospheric perturbations, *Geophys. Res. Lett.*, *32*, L08804, doi:10.1029/2004GL022187.
- Cheng, Z., S. A. Cummer, D. N. Baker, and S. G. Kanekal (2006), Nighttime D region electron density profiles and variabilities inferred from broadband measurements using VLF radio emissions from lightning, *J. Geophys. Res.*, *111*, A05302, doi:10.1029/2005JA011308.
- Clemmow, P. C., and J. Heading (1954), Coupled forms of the differential equations governing radio propagation in the ionosphere, *Math. Proc. Cambridge Philos. Soc.*, *50*(2), 319, doi:10.1017/s030500410002939x.
- Cummer, S. A. (2000), Modeling electromagnetic propagation in the Earth-ionosphere waveguide, *IEEE Trans. Antennas Propag.*, *48*(9), 1420–1429.
- Cummer, S. A., and U. S. Inan (2000), Ionospheric E region remote sensing with ELF radio atmospherics, *Radio Sci.*, *35*, 1437–1444, doi:10.1029/2000RS002335.
- Cummer, S. A., U. S. Inan, and T. F. Bell (1998), Ionospheric D region remote sensing using VLF radio atmospherics, *Radio Sci.*, *33*, 1781–1792, doi:10.1029/98RS02381.

- Davies, K. (1990), *Ionospheric Radio*, Peter Peregrinus Ltd., London.
- Ferguson, J. A., F. P. Snyder, D. G. Morfitt, and C. H. Shellman (1989), *Long-Wave Propagation Capability and Documentation*, Tech. Doc., edited by Naval Ocean System Center, Naval Ocean Systems Center, San Diego, Calif.
- Fock, V. A. (1965), *Electromagnetic Diffraction and Propagation Problems*, Pergamon Press, New York.
- Galejs, J. (2013), *Terrestrial Propagation of Long Electromagnetic Waves: International Series of Monographs in Electromagnetic Waves*, Elsevier, Oxford.
- Graf, K., M. Spasojevic, R. Marshall, N. Lehtinen, F. Foust, and U. Inan (2013), Extended lateral heating of the nighttime ionosphere by ground-based VLF transmitters, *J. Geophys. Res. Space Physics*, *118*, 7783–7797, doi:10.1002/2013JA019337.
- Haddad, M. A., V. A. Rakov, and S. A. Cummer (2012), New measurements of lightning electric fields in Florida: Waveform characteristics, interaction with the ionosphere, and peak current estimates, *J. Geophys. Res.*, *117*, D10101, doi:10.1029/2011JD017196.
- Han, F., and S. A. Cummer (2010a), Midlatitude daytime D region ionosphere variations measured from radio atmospherics, *J. Geophys. Res.*, *115*, A10314, doi:10.1029/2010JA015715.
- Han, F., and S. A. Cummer (2010b), Midlatitude nighttime D region ionosphere variability on hourly to monthly time scales, *J. Geophys. Res.*, *115*, A09323, doi:10.1029/2010JA015437.
- Han, F., S. A. Cummer, J. Li, and G. Lu (2011), Daytime ionospheric D region sharpness derived from VLF radio atmospherics, *J. Geophys. Res.*, *116*, A05314, doi:10.1029/2010JA016299.
- Hu, W., and S. A. Cummer (2006), An FDTD model for low and high altitude lightning-generated EM fields, *IEEE Trans. Antennas Propag.*, *54*(5), 1513–1522.
- Inoue, Y., and S. Horowitz (1966), Numerical solution of full-wave equation with mode coupling, *Radio Sci.*, *1*, 957–970, doi:10.1002/rds196618957.
- ITURP (1999), *832–2, World Atlas of Ground Conductivities*, ITU, Geneva.
- ITURP (2002), *684–3, Prediction of Field Strength at Frequencies Below 150 kHz*, ITU, Geneva.
- Jacobson, A. R., X.-M. Shao, and R. Holzworth (2009), Full-wave reflection of lightning long-wave radio pulses from the ionospheric D region: Numerical model, *J. Geophys. Res.*, *114*, A03303, doi:10.1029/2008JA013642.
- Jacobson, A. R., X.-M. Shao, and E. H. Lay (2012), Time domain waveform and azimuth variation of ionospherically reflected VLF/LF radio emissions from lightning, *Radio Sci.*, *47*, RS4001, doi:10.1029/2012RS004980.
- Johler, J. R., and J. D. Harper Jr. (1962), Reflection and transmission of radio waves at a continuously stratified plasma with arbitrary magnetic induction, *J. Res. NBS Radio Propag.*, *66D*, 81–99.
- Lay, E. H., and X.-M. Shao (2011a), High temporal and spatial-resolution detection of D-layer fluctuations by using time-domain lightning waveforms, *J. Geophys. Res.*, *116*, A01317, doi:10.1029/2010JA016018.
- Lay, E. H., and X.-M. Shao (2011b), Multi-station probing of thunderstorm-generated D-layer fluctuations by using time-domain lightning waveforms, *Geophys. Res. Lett.*, *38*, L23806, doi:10.1029/2011GL049790.
- Lay, E. H., X. M. Shao, and A. R. Jacobson (2014), D region electron profiles observed with substantial spatial and temporal change near thunderstorms, *J. Geophys. Res. Space Physics*, *119*, 4916–4928, doi:10.1002/2013JA019430.
- Lehtinen, N. G., and U. S. Inan (2008), Radiation of ELF/VLF waves by harmonically varying currents into a stratified ionosphere with application to radiation by a modulated electrojet, *J. Geophys. Res.*, *113*, A06301, doi:10.1029/2007JA012911.
- Lehtinen, N. G., and U. S. Inan (2009), Full-wave modeling of transionospheric propagation of VLF waves, *Geophys. Res. Lett.*, *36*, L03104, doi:10.1029/2008GL036535.
- Marshall, R. A. (2012), An improved model of the lightning electromagnetic field interaction with the D-region ionosphere, *J. Geophys. Res.*, *117*, A03316, doi:10.1029/2011JA017408.
- Marshall, R. A., and U. S. Inan (2010), Two-dimensional frequency domain modeling of lightning EMP-induced perturbations to VLF transmitter signals, *J. Geophys. Res.*, *115*, A00E29, doi:10.1029/2009JA014761.
- Nagano, I., M. Mambo, and G. Hutatsuishi (1975), Numerical calculation of electromagnetic waves in an anisotropic multilayered medium, *Radio Sci.*, *10*, 611–617, doi:10.1029/RS010i006p00611.
- Nagano, I., S. Yagitani, K. Miyamura, and S. Makino (2003), Full-wave analysis of elves created by lightning-generated electromagnetic pulses, *J. Atmos. Sol. Terr. Phys.*, *65*(5), 615–625.
- Pal, S. (2015), Numerical modelling of VLF radio wave propagation through Earth-ionosphere waveguide and its application to sudden ionospheric disturbances.
- Pavlov, A. V. (2013), Photochemistry of ions at D-region altitudes of the ionosphere: A review, *Surv. Geophys.*, *35*(2), 259–334, doi:10.1007/s10712-013-9253-z.
- Pitteway, M. L. (1965), The numerical calculation of wave-fields, reflexion coefficients and polarizations for long radio waves in the lower ionosphere. I, *Philos. Trans. R. Soc. London Ser. A*, *257*(1079), 219–241.
- Price, G. H. (1964), Propagation of electromagnetic waves through a continuously varying stratified anisotropic medium, *Radio Sci. J. Res.*, *68D*, 407–418.
- Qin, Z. (2014), *The Observation of Ionospheric D-layer based on the Multi-station Lightning Detection System* [in Chinese], Univ. of Sci. and Technol. of China, Hefei.
- Qin, Z., B. Zhu, F. Lyu, M. Ma, and D. Ma (2015), Using time domain waveforms of return strokes to retrieve the daytime fluctuation of ionospheric D layer (in Chinese), *Chinese Sci. Bull.*, *7*, 654–663, doi:10.1360/N972014-00223.
- Shao, X.-M., and A. R. Jacobson (2009), Model simulation of very low-frequency and low-frequency lightning signal propagation over intermediate ranges, *IEEE Trans. Electromagn. Compat.*, *51*(3), 519–525.
- Shao, X.-M., M. Stanley, A. Regan, J. Harlin, M. Pongratz, and M. Stock (2006), Total lightning observations with the new and improved Los Alamos Sferic Array (LASA), *J. Atmos. Oceanic Technol.*, *23*(10), 1273–1288.
- Shao, X.-M., E. H. Lay, and A. R. Jacobson (2012), Reduction of electron density in the night-time lower ionosphere in response to a thunderstorm, *Nat. Geosci.*, doi:10.1038/ngeo1668.
- Thébault, E., C. C. Finlay, C. D. Beggan, P. Alken, J. Aubert, O. Barrois, F. Bertrand, T. Bondar, A. Boness, and L. Brocco (2015), International geomagnetic reference field: The 12th generation, *Earth Planets Space*, *67*(1), 1–19.
- Thomson, N. R. (2004), Ionosphere gives size of greatest solar flare, *Geophys. Res. Lett.*, *31*, L06803, doi:10.1029/2003GL019345.
- Thomson, N. R. (2005), Large solar flares and their ionospheric D-region enhancements, *J. Geophys. Res.*, *110*, A06306, doi:10.1029/2005JA011008.
- Thomson, N. R. (2010), Daytime tropical D region parameters from short path VLF phase and amplitude, *J. Geophys. Res.*, *115*, A09313, doi:10.1029/2010JA015355.
- Thomson, N. R., and M. A. Clilverd (2000), Solar cycle changes in daytime VLF subionospheric attenuation, *J. Atmos. Sol. Terr. Phys.*, *62*(7), 601–608.

- Thomson, N. R., and W. M. McRae (2009), Nighttime ionospheric *D*-region: Equatorial and nonequatorial, *J. Geophys. Res.*, *114*, A08305, doi:10.1029/2008JA014001.
- Thomson, N. R., M. A. Clilverd, and W. M. McRae (2007), Nighttime ionospheric *D*-region parameters from VLF phase and amplitude, *J. Geophys. Res.*, *112*, A07304, doi:10.1029/2007JA012271.
- Wait, J. R. (1961), A diffraction theory for LF sky-wave propagation, *J. Geophys. Res.*, *66*, 1713–1724, doi:10.1029/JZ066i006p01713.
- Wait, J. R. (2013), *Electromagnetic Waves in Stratified Media: Revised Edition Including Supplemented Material*, Elsevier, Oxford.
- Wait, J. R., and K. P. Spies (1964), *Characteristics of the Earth-ionosphere Waveguide for VLF Radio Waves*, US Dep. of Commerce, National Bureau of Standards, Boulder, Colo.
- Zhao, S., X. Shen, W. Pan, X. Zhang, and L. Liao (2010), Penetration Characteristics of VLF Wave From Atmosphere Into Lower Ionosphere, *Earthquake Sci.*, *23*(3), 275–281.